

1 **Fossil vs. non-fossil sources of fine carbonaceous**
2 **aerosols in four Chinese cities during the extreme**
3 **winter haze episode in 2013**

4
5 **Yan-Lin Zhang^{1,2,3,4,*}, Ru-Jin Huang², Imad El Haddad², Kin-Fai Ho^{5,6}, Jun-Ji**
6 **Cao⁶, Yongming Han⁶, Peter Zotter², Carlo Bozzetti², Kaspar R. Daellenbach²,**
7 **Francesco Canonaco², Jay G. Slowik², Gary Salazar^{1,3}, Margit Schwikowski^{2,3},**
8 **Jürgen Schnelle-Kreis⁷, Gülcin Abbaszade⁷, Ralf Zimmermann^{7,8}, Urs**
9 **Baltensperger², Andr  s.H. Pr  v  t², S  nke Szidat^{1,3,*}**

10 ¹Department of Chemistry and Biochemistry, University of Bern, Freiestrasse 3, 3012 Bern,
11 Switzerland

12 ²Paul Scherrer Institute (PSI), Villigen, 5232 Villigen-PSI, Switzerland

13 ³Oeschger Centre for Climate Change Research, University of Bern, 3012 Bern, Switzerland

14 ⁴Yale-NUIST Center on Atmospheric Environment, Nanjing University of Information
15 Science and Technology, Nanjing, Jiangsu, China

16 ⁵School of Public Health and Primary Care, The Chinese University of Hong Kong, Hong
17 Kong, China

18 ⁶Key Lab of Aerosol Science & Technology, SKLLQG, Institute of Earth Environment,
19 Chinese Academy of Sciences, Xi'an, 710075, China

20 ⁷Helmholtz Zentrum M  nchen, German Research Center for Environmental Health (GmbH),
21 Joint Mass Spectrometry Centre, Cooperation Group Comprehensive Molecular Analytics
22 and Helmholtz Virtual Institute of Complex Molecular Systems in Environmental Health —
23 Aerosol and Health (HICE), 85764 Neuherberg, Germany.

24 ⁸University of Rostock, Joint Mass Spectrometry Centre, Institute of Chemistry – Chair of
25 Analytical Chemistry, 18015 Rostock, Germany

26
27 *Correspondence to dryanlinzhang@gmail.com (Y. L. Zhang); szidat@dcb.unibe.ch (S.
28 Szidat)

29 **Abstract**

30 During winter 2013, extremely high concentrations (i.e. 4-20 times higher than the World
31 Health Organization guideline) of PM_{2.5} (particulate matter with an aerodynamic diameter <2.5
32 μm) mass concentrations (24 hour samples) were found in four major cities in China including
33 Xian, Beijing, Shanghai and Guangzhou. Statistical analysis of a combined dataset from
34 elemental carbon (EC) and organic carbon (OC), ¹⁴C and biomass-burning marker measurements
35 using Latin-hypercube sampling allowed a quantitative source apportionment of carbonaceous
36 aerosols. Based on ¹⁴C measurement in EC fraction (6 samples each city), we found that fossil
37 emissions from coal combustion and vehicle exhaust dominated EC with a mean contribution of
38 75±8% across all sites. The remaining 25±8% was exclusively attributed to biomass combustion,
39 consistent with the measurements of biomass-burning markers such as anhydrosugars
40 (levoglucosan and mannosan) and water-soluble potassium (K⁺). With a combination of the
41 levoglucosan-to-mannosan and levoglucosan-to-K⁺ ratios, the major source of biomass burning in
42 winter in China is suggested to be combustion of crop residues. The contribution of fossil sources
43 to OC was highest in Beijing (58±5%) and decreased from Shanghai (49±2%) to Xian (38±3%)
44 and Guangzhou (35±7%). Generally, a larger fraction of fossil OC was from secondary origins
45 than primary sources for all sites. Non-fossil sources accounted on average for 55±10% and
46 48±9% of OC and TC, respectively, which suggests that non-fossil emissions were very important
47 contributors of urban carbonaceous aerosols in China. The primary biomass-burning emissions
48 accounted for 40±8%, 48±18%, 53±4% and 65±26% of non-fossil OC for Xian, Beijing,
49 Shanghai and Guangzhou, respectively. Other non-fossil sources excluding primary biomass-
50 burning were mainly attributed to formation of secondary organic carbon (SOC) from non-fossil
51 precursors such as biomass-burning emissions. For each site, we also compared samples from
52 moderately with heavily polluted days according to particulate matter mass. Despite a significant
53 increase of absolute mass concentrations of primary emissions from both fossil and non-fossil
54 sources during the heavily polluted events, their relative contribution to TC was even decreased,
55 whereas the portion of SOC was consistently increased at all sites. This observation indicates that
56 SOC was an important fraction in the increment of carbonaceous aerosols during the haze episode
57 in China.

58 **1 Introduction**

59 Driven by continuous urbanization and industrialization and a rapid growth in the number of
60 motor vehicles and energy consumption, large-scale severe air pollution episodes often affect
61 most cities in China. An increase in the number of haze days is expected to have an adverse
62 impact on human health (Chan and Yao, 2008). Atmospheric fine particles such as PM_{2.5}
63 (particulate matter with an aerodynamic diameter of below 2.5 μm) have been reported as an
64 important air pollutant in China (Donkelaar et al., 2010; Yang et al., 2011; Cao et al., 2012;
65 Huang et al., 2013; Zhao et al., 2013), and its burden is much higher than the 24h-mean of 25
66 μg/m³ suggested by the Air Quality Guidelines of the of World Health Organization (WHO)
67 (WHO, 2006).

68 Carbonaceous aerosols are a major fraction of PM_{2.5} contributing 20-50% of the total PM
69 mass in China's urban atmosphere (Cao et al., 2007). In addition to health and visibility effects,
70 carbonaceous aerosols also influence the earth's climate directly by scattering and absorbing solar
71 radiation and indirectly by modifying cloud microphysics (Pöschl, 2005; IPCC, 2013).
72 Carbonaceous aerosols can be classified into elemental carbon (EC) and organic carbon (OC). EC
73 is exclusively emitted as primary aerosols from incomplete combustion of fossil fuels and
74 biomass burning, whereas OC is a complex mixture of primary directly emitted OC particles
75 (POC) and secondary OC (SOC) formed in-situ in the atmosphere via the oxidation of gas-phase
76 precursors (Pöschl, 2005). POC and precursors of SOC may stem from a vast variety of sources
77 from both anthropogenic (e.g. coal combustion, vehicle emissions and cooking) and natural
78 sources (e.g. biogenic emissions) (Carlton et al., 2009). These sources change over time and
79 space, which makes source apportionment difficult.

80 Several techniques have been applied to quantify the emission sources of carbonaceous
81 aerosols. Radiocarbon (¹⁴C) measurements provide a powerful tool for unambiguously
82 determining fossil and non-fossil sources of carbonaceous particles, since ¹⁴C is completely
83 depleted in fossil-fuel emissions due to its age (half-life 5730 years), whereas non-fossil carbon
84 sources (e.g. biomass burning, cooking or biogenic emissions) show a contemporary ¹⁴C content
85 (Szidat, 2009; Heal, 2014). Moreover, a better ¹⁴C-based source apportionment can be obtained
86 when ¹⁴C determinations are performed on OC and EC separately, since EC originates exclusively
87 from combustion of biomass and fossil fuels (Szidat et al., 2006; Szidat, 2009; Bernardoni et al.,
88 2013; Liu et al., 2013; Zhang et al., 2013). However, as both biogenic and biomass-burning OC
89 contain ¹⁴C on the contemporary level, it is still difficult to quantify the contribution from these
90 two sources to OC by ¹⁴C measurements alone. When these are combined with OC/EC and

91 organic marker measurements, the primary and secondary origins of the fossil and non-fossil
92 fractions can be identified (Szidat et al., 2006; Szidat et al., 2007; Szidat et al., 2009; Minguillón
93 et al., 2011; Yttri et al., 2011). In particular, levoglucosan, a thermal degradation product of
94 cellulose combustion, can be used as molecular marker to identify primary biomass-burning
95 emissions (Simoneit et al., 1999; Puxbaum et al., 2007; Viana et al., 2013).

96 During January 2013, the severe problem of air pollution in China became a worldwide
97 concern, as extremely high concentrations of 24-h PM_{2.5} (i.e. often >100 µm³) were reported
98 in several large cities affecting ~1.3 million km² and ~800 million people. To investigate sources
99 and formation mechanisms of fine carbonaceous aerosols from this high pollution episode across
100 China, an intensive field experiment was carried out in the four large cities Xian, Beijing,
101 Shanghai and Guangzhou, each of them located in different climatic regions, i.e. central-
102 northwest region, Beijing-Tianjin region, Yangtze Delta Region, and Pearl River Delta Region,
103 respectively. These measurements were used in conjunction with Latin-hypercube sampling
104 (LHS) (Gelencsér et al., 2007), to elucidate the origins of the carbonaceous aerosol during the
105 haze event.

106 **2 Methods**

107 **2.1 Sampling**

108 Measurement sites are located in Xian, Beijing, Shanghai and Guangzhou, the representative
109 cities of the central-northwest region, Beijing-Tianjin region, Yangtze Delta Region, and Pearl
110 River Delta Region, respectively. In these regions, haze events frequently occur during winter,
111 when weather conditions trap pollutants over the plain. Detailed descriptions of the sampling sites
112 are given in Table 1. In each city, 24-hour integrated PM_{2.5} samples were collected on pre-baked
113 quartz filters using high-volume samplers at a flow rate of ~1.05 m³/min from 5 to 25 January
114 2013. The sampling sites are located within campuses of universities or at research centers, >100
115 m away from local sources, such as major roadways, industry or domestic sources. At each
116 sampling site, one field blank sample was collected and analyzed. The results reported here are
117 corrected for corresponding field blanks (Cao et al., 2013). All samples collected were stored at -
118 20 °C before analysis. The PM_{2.5} mass on each filter was gravimetrically measured using a
119 temperature and relative humidity controlled microbalance.

120 **2.2 Thermal-optical carbon analysis**

121 A 1.0 cm² punch from the filter samples is taken for the analysis of the OC and EC mass
122 concentrations by the EUSAAR_2 thermal-optical transmission protocol (Cavalli et al., 2010).
123 The replicate analysis of samples (n = 6) showed a good analytical precision with relative
124 standard deviations of 4.8%, 9.1%, and 5.0% for OC, EC and TC, respectively. The average field
125 blank of OC was 2.0 ± 1.0 µg/cm² (equivalent to ~0.5 µg/m³), which was subtracted from the
126 measured OC concentrations. A corresponding EC blank was not detectable.

127 **2.3 ¹⁴C analysis of the carbonaceous fractions**

128 Six filters were selected per sampling site for ¹⁴C analysis, three from days with a very high
129 PM loading and three representing an average loading, which are described in Table S1 in the
130 supplement. A thermo-optical OC/EC analyzer (Model4L, Sunset Laboratory Inc, USA) equipped
131 with a non-dispersive infrared (NDIR) detector is used for the isolation of different carbon
132 fractions for subsequent ¹⁴C measurements using a four-step thermo-optical protocol Swiss_4S.
133 The method is described in detail elsewhere (Zhang et al., 2012). For EC isolation, filter samples
134 are first treated by water extraction to remove water-soluble OC to minimize the positive artefact
135 from OC charring to the ¹⁴C result of EC. To remove both non-refractory and refractory OC
136 fractions, the water-extracted filters are then combusted or heated in the following 3 steps: step 1
137 in an oxidizing atmosphere (O₂, 99.9995%) at 375 °C for 150s; step 2 in O₂ at 475 °C for 180s;
138 step 3 in helium, at 450 °C for 180s followed by at 650 °C for 180s. Finally, EC is isolated by the
139 combustion of the remaining carbonaceous material at 760 °C within 150s in O₂. This method is
140 optimized to minimize a possible negative EC artifact due to losses of the least refractory EC in
141 the OC removal steps prior to EC collection. In a recent study, we found that the aforementioned
142 negative artefact due to premature EC loss during a harsh OC removal procedure (e.g.
143 combustion of samples at 375 °C for 4 h or longer) before EC isolation potentially underestimates
144 biomass-burning EC contribution by up to ~70%, if only small amounts of EC are recovered
145 (Zhang et al., 2012). The EC recovery for ¹⁴C measurement in this work is 78±10%. A bias from
146 underestimation of biomass burning EC caused by the EC loss of 22 ±10% is corrected using the
147 approach described by Zhang et al. (2012). For TC samples, the filters are combusted using the
148 whole Swiss_4S protocol without OC/EC separation. After the combustion/separation of the
149 desired carbonaceous aerosol fractions (i.e. TC or EC), the resulting CO₂ is trapped cryogenically
150 and sealed in glass ampoules for ¹⁴C measurement, which is conducted by a tabletop accelerator
151 mass spectrometry (AMS) system MICADAS using a gas ion source (Wacker et al., 2013) at the

152 Laboratory for the Analysis of Radiocarbon with AMS (LARA), University of Bern, Switzerland
153 (Szidat et al., 2014). ^{14}C results are expressed as fractions of modern (f_M), i.e. the fraction of the
154 $^{14}\text{C}/^{12}\text{C}$ ratio of the sample related to the isotopic ratio of the reference year 1950 (Stuiver and
155 Polach, 1977). This data is then corrected for ^{14}C decay during the period between 1950 and
156 2013, i.e. the year of measurement. The uncertainties of $f_M(\text{EC})$ and $f_M(\text{TC})$ are <5% and <2%,
157 respectively. ^{14}C results in OC ($f_M(\text{OC})$) is not measured directly, but calculated by:

$$158 \quad f_M(\text{OC}) = \frac{\text{TC} \times f_M(\text{TC}) - \text{EC} \times f_M(\text{EC})}{\text{OC}} \quad (1)$$

159 The uncertainty of $f_M(\text{OC})$ estimated by this approach is on average 8% obtained from an
160 error propagation and include all the individual uncertainties of the $f_M(\text{TC})$ (2%), $f_M(\text{EC})$ (5%),
161 TC (8%) and EC (25%). No blank corrections are made for determination of ^{14}C , as the different
162 carbonaceous fractions contributions from field blanks are all less than 2% and thus can be
163 neglected.

164 **2.4 Anhydrosugars and water-soluble potassium measurements**

165 The anhydrosugars (levoglucosan and mannosan) are measured by a recently developed in-
166 situ derivatization/thermal desorption gas-chromatography-mass spectrometry method (IDTD-
167 GC-MS) (Schnelle-Kreis et al., 2005; Orasche et al., 2011). Briefly, the filter punches are placed
168 into glass liners suitable for an automated thermal desorption unit. Isotope-labelled standard
169 compounds are spiked onto the filter surface to account for matrix-influences for quantification.
170 Derivatization is performed on the filter by adding of liquid reagent N-methyl-N-(trimethylsilyl)
171 trifluoroacetamide (MSTFA, Macherey-Nagel, Germany). During 16 min of desorption time, in
172 addition an in-situ derivatization with gaseous MSTFA is carried out to quantitatively silylate
173 polar organic compounds and optimize the automated desorption process. Derivatized and
174 desorbed molecules are first trapped on a pre-column before separation by gas chromatography
175 (BPX-5 capillary column, SGE, Australia). The detection and quantification of compounds is
176 carried out on a Pegasus III time-of-flight mass spectrometer (TOF-MS) using the ChromaTOF
177 software package (LECO, St. Joseph, MI).

178 Concentrations of water-soluble potassium (K^+) and other ions are analyzed with ion
179 chromatography (850 Professional IC, Metrohm, Switzerland) after leaching of a 1.0 cm^2 punch
180 of the filter samples with 50 g of ultrapure water (18.2 $\text{M}\Omega$ quality) for 30 min at 40°C in an
181 ultrasonic bath.

182 2.5 Source apportionment methodology

183 Source apportionment results are obtained by Latin-hypercube sampling (LHS) using the
184 dataset from the measured OC, EC, and levoglucosan mass concentrations, estimated emission
185 ratios as well as ¹⁴C contents of OC and EC. The LHS methodology which is comparable to
186 Monte Carlo simulation was first proposed by (Gelencsér et al., 2007) and later applied in many
187 European sites (e.g. Szidat et al. (2009), Yttri et al. (2011), Gilardoni et al. (2011) and Genberg et
188 al. (2011)). Briefly, central values with low and high limits are associated to all uncertain input
189 parameters (Table 2). Due to the lack of information on the input factors, parameters are assigned
190 equally between the low limit and the central value and between the central value and the high
191 limit. All combinations of parameters are included in frequency distributions of possible solutions
192 except those producing negative values. The approach used here is slightly modified compared to
193 previous studies and briefly summarized in the following.

194 EC arises from biomass burning (EC_{bb}) and fossil-fuel combustion (EC_f):

$$195 \quad EC = EC_f + EC_{bb} \quad (2)$$

196 EC_{bb} is calculated from the EC mass concentration, f_M(EC) and a reference value of biomass-
197 burning EC (i.e. fraction of modern in EC emitted from biomass-burning sources, f_M(bb):

$$198 \quad EC_{bb} = EC \times \frac{f_M(EC)}{f_M(bb)} \quad (3)$$

199 Analogously, OC is divided into two sub-fractions, OC from fossil fuel (OC_f) and non-fossil
200 emissions (OC_{nf}). To account for the thermonuclear weapon tests of the late 1950s and early
201 1960s, OC_{nf} is calculated from the OC mass concentration, f_M(OC) and a ¹⁴C reference value of
202 non-fossil emissions (i.e. fraction of modern in OC emitted from non-fossil sources, f_M(nf)). :

$$203 \quad OC = OC_f + OC_{nf} \quad (4)$$

$$204 \quad OC_{nf} = OC \times \frac{f_M(OC)}{f_M(nf)} \quad (5)$$

205 In addition to this straightforward OC distinction, OC_f and OC_{nf} are semi-quantitatively
206 classified into additional sub-fractions. On the one hand, OC_f is split into primary and secondary
207 OC from fossil sources, i.e. OC_{pri,f} and OC_{sec,f}, respectively:

$$208 \quad OC_f = OC_{pri,f} + OC_{sec,f} \quad (6)$$

209 OC_{pri,f} is determined from EC_f and a primary OC/EC emission ratio for fossil-fuel
210 combustion, i.e. (OC/EC)_{pri,f}:

$$211 \quad OC_{pri,f} = EC_f \times \left(\frac{OC}{EC} \right)_{pri,f} \quad (7)$$

212 As fossil-fuel combustion in China is almost exclusively from coal combustion and vehicle
213 emissions, (OC/EC)_{pri,f} can be determined as:

$$\left(\frac{OC}{EC}\right)_{pri,f} = p \times \left(\frac{OC}{EC}\right)_{pri,cc} + (1 - p) \times \left(\frac{OC}{EC}\right)_{pri,ve} \quad (8)$$

214 where p is a percentage of coal combustion in total fossil emissions, and $(OC/EC)_{pri,cc}$ and
 215 $(OC/EC)_{pri,ve}$ a primary OC/EC ratio for coal combustion (cc) and vehicle emissions (ve),
 216 respectively.

217 This strategy can only be applied to OC_{nf} after some modification, as its primary OC/EC
 218 emission ratio is far too uncertain for a general split of non-fossil OC into of primary vs.
 219 secondary formation. Alternatively, OC_{nf} is subdivided into primary biomass burning (OC_{bb}) and
 220 all the other non-fossil sources ($OC_{other,nf}$):

$$OC_{nf} = OC_{bb} + OC_{other,nf} \quad (9)$$

222 $OC_{other,nf}$ includes all the other non-fossil sources except OC_{bb} , thus mainly representing
 223 primary and secondary biogenic OC, urban non-fossil contributions (e.g. from cooking or frying)
 224 as well as SOC from biomass burning; due to cholesterol concentrations below the limit of
 225 detection in all samples, however, contributions of cooking and/or frying to $OC_{other,nf}$ can be
 226 neglected. OC_{bb} is calculated by two alternative “marker-to-OC” methods using either EC_{bb} or
 227 levoglucosan (lev) as biomass-burning marker with corresponding primary marker-to-OC
 228 emission ratios (Eq. 9 and 10).

$$OC_{bb} = \frac{EC_{bb}}{\left(\frac{EC}{OC}\right)_{bb}} \quad (10)$$

$$OC_{bb} = \frac{lev}{\left(\frac{lev}{OC}\right)_{bb}} \quad (11)$$

230 The overlapping results of both calculations are considered as probable solutions for OC_{bb} .
 231 The consistency of EC_{bb} and levoglucosan data is shown below in Figure 4.

232 Extensive discussion of the selection of the used input parameters can be found in earlier
 233 studies conducted in Europe (e.g. (Gelencsér et al., 2007), (Szidat et al., 2009), (Yttri et al., 2011),
 234 (Gilardoni et al., 2011), (Genberg et al., 2011)). However, due to different conditions in this study,
 235 the input values have to be adapted (Table 2):

- 236 I. To correct for the ^{14}C bomb peak, the reference values of f_M for biomass burning and non-
 237 fossil sources, i.e. $f_M(bb)$ and $f_M(nf)$, respectively, are adapted to the sampling year 2013.
 238 $f_M(bb)$ is estimated as 1.10 ± 0.05 using a tree growth model as described in (Mohn et al.,
 239 2008). The low limit of $f_M(nf)$ is 1.03, which is equal to the f_M of CO_2 in the atmosphere
 240 (Levin et al., 2010), and the high limit of $f_M(nf)$ is set to $f_M(bb)$ with the central value as
 241 the average of both.

242 II. Literature data indicate that emission ratios depend on fuel types and combustion
 243 conditions as well as specific measurement techniques, e.g. for EC mass (Fine et al.,
 244 2004; Puxbaum et al., 2007). A range of 0.07-0.20 and 0.10-0.30 is used as the low-to-
 245 high values for the $(\text{lev}/\text{OC})_{\text{bb}}$ and $(\text{EC}/\text{OC})_{\text{bb}}$, respectively, covering most of the variation
 246 in the measurements and the range used in previous studies (e.g. Gelencser et al. (2007);
 247 Genberg et al. (2011); Szidat et al. (2009); Yttri et al. (2011)). Zhang et al. (2007b)
 248 reported an average $(\text{lev}/\text{OC})_{\text{bb}}$ ratio of 0.082 for the main types of Chinese cereal straw
 249 (rice, wheat, and corn) based on combustion chamber experiments. As cereal straw is one
 250 of the most abundant biomass burned in China, the above ratio (0.082) was used to
 251 estimate biomass-burning contribution to OC in Beijing (Zhang et al., 2008) and Hong
 252 Kong (Sang et al., 2011). However, this ratio is lower than that (0.14) obtained from the
 253 combustion of hardwood in fireplaces and stoves in the US (Fine et al., 2004), which was
 254 applied to estimate the contribution of biomass burning to OC at background sites in
 255 Europe (Gelencsér et al., 2007; Puxbaum et al., 2007; Schmidl et al., 2008). Considering
 256 both main biomass types (i.e. mainly cereal-straw, but also hard-wood burning) (see Sec.
 257 3.2.3), the central value for $(\text{lev}/\text{OC})_{\text{bb}}$ of 0.11 is used in this study. Based on emission
 258 factors for primary particulate emissions in China (Zhang et al., 2007), the central value
 259 for $(\text{EC}/\text{OC})_{\text{bb}}$ is chosen as 0.22.

260 III. $(\text{EC}/\text{OC})_{\text{pri,ve}}$ is determined for emissions from traffic as 0.8-2.1 with the central value of
 261 1.45, which is taken from composite profiles from tunnel experiments in Europe
 262 (Gelencsér et al., 2007) and the range of this ratio also covers many tunnel studies
 263 conducted in China (Huang et al., 2006; He et al., 2008). For $(\text{EC}/\text{OC})_{\text{pri,cc}}$, it ranges for
 264 emissions for coal burning in China from 0.32 to 0.62 depending on the share of briquette
 265 and chunk bituminous coal with central value of 0.44 for the average coal inventory (Zhi
 266 et al., 2008).

267 IV. In many urban sites such as Barcelona (Minguillón et al., 2011), Zurich (Szidat et al.,
 268 2006) and Pasadena (Zotter et al., 2014), EC_f was almost exclusively attributed to vehicle
 269 emissions. However, in China coal combustion is also considered to be an important
 270 contributor to EC emission in winter from both field studies (Cao et al., 2011b) and
 271 inventory estimations (Cao et al., 2011a). Recently, Huang et al. (2014) reported relative
 272 contribution from coal combustion to total fossil emissions (i.e. p in the Eq (8)) ranges
 273 from 0.16-0.80 in Chinese aerosols. In this study, p is assigned as 0-0.7 with the central
 274 value of 0.35. It should be noted that for the regions with negligible coal combustion, p

275 can be directly assigned as 0 to simplify this approach. In such a case, $(EC/OC)_{pri,f}$ is
276 equal to $(EC/OC)_{pri,ve}$.

277 To evaluate uncertainties of the quantification of source contributions, the LHS method is
278 implemented to generate 3000 random sets of variables (Gelencsér et al., 2007). A few
279 simulations producing negative solutions are excluded and the median value from the remaining
280 simulations is considered as the best estimate (see Sec 3.2), and the 10th and 90th percentiles of the
281 solutions are treated as uncertainties. These uncertainties typically amount to 13% and 10% for
282 the separation of EC into EC_f and EC_{bb} as well as for OC into OC_f and OC_{nf} , respectively. The
283 uncertainties are higher for the further source apportionment of OC (on the average 25%, 20%,
284 20% and 25% for $OC_{pri,f}$, $OC_{sec,f}$, OC_{bb} and $OC_{other,nf}$, respectively). The ¹⁴C analysis performed on
285 the EC fraction directly enables a more reliable quantification of fossil and biomass burning EC
286 compared to those results obtained by many previous studies (e.g. Gelencser et al., 2007; Yttri et
287 al., 2011; Genberg et al., 2011), in which ¹⁴C analysis were only conducted on TC samples alone.
288 The results of the sensitivity analysis and the determination of the uncertainties will be discussed
289 further in Sec. 3.2.4. The comparison of the ¹⁴C approach with other organic makers (see Sec
290 3.2.3) as well as with the source apportionment results from positive matrix factorization (Paatero
291 and Tapper, 1994) using the multi-linear engine (ME-2) algorithm (Paatero and Hopke, 2009)
292 (see Sec. 3.3.3) will provide additional measures to evaluate the model performance.

293 **3 Results and discussions**

294 **3.1 PM2.5 and carbonaceous aerosols mass concentrations**

295 The whisker box plots (Figure 1) show the concentrations of PM2.5, OC and EC as well as
296 EC to OC ratios (EC/OC) in the four Chinese cities. The average PM2.5 mass concentrations at
297 the Xian, Beijing, Shanghai, and Guangzhou sampling sites during the sampling periods were
298 $345 \pm 125 \mu\text{g}/\text{m}^3$, $158 \pm 81 \mu\text{g}/\text{m}^3$, $90 \pm 31 \mu\text{g}/\text{m}^3$, and $68 \pm 23 \mu\text{g}/\text{m}^3$, respectively. Despite large
299 variations in the PM2.5 concentrations within each site, their concentrations were always higher
300 in Xian and Beijing compared to those in Shanghai and Guangzhou, reflecting a poorer air quality
301 in Northern China. Extremely high PM2.5 concentrations were observed for several days during
302 the sampling period. The highest 24-h average PM2.5 value ($134\text{-}517 \mu\text{g}/\text{m}^3$) was 5-20 times
303 higher than the WHO guideline for 24-h PM2.5 ($25 \mu\text{g}/\text{m}^3$, (WHO, 2006)). Only 3% of PM2.5
304 mass values were below this guideline value, indicating a very high negative impact on human
305 health in all studied cities.

306 OC and EC concentrations showed similar spatial distributions as the PM_{2.5} mass in the
307 order: Xian>Beijing>Shanghai>Guangzhou. Given that average temperatures during the sampling
308 period were 10-20°C lower in Xian and Beijing than in Shanghai and Guangzhou, the high
309 concentrations of carbonaceous species in northern cities could be due to enhanced fuel
310 consumption for heating activities (Weilenmann et al., 2009; Nordin et al., 2013). The EC/OC
311 ratios were comparable for Xian, Shanghai and Guangzhou, but considerably lower at Beijing.

312 We also compared the data of OC, EC and EC/OC from heavily polluted days with
313 moderately polluted days, which were selected from the samples with the highest and average PM
314 loading, respectively (Table 3). ¹⁴C measurements were also performed on these samples (Sect.
315 2.3), and a detailed source apportionment result will be presented in Sect. 3.2. The PM_{2.5}, OC
316 and EC mass concentrations on heavily polluted days were mostly >2 times as high as those on
317 moderately polluted days at the four sites. On the heavily polluted days, the EC/OC ratios
318 significantly decreased by 29% and 43% in northern cities of Xian and Beijing, respectively,
319 whereas they slightly increased in Shanghai and Guangzhou by 13% and 16%, respectively. [The
320 higher PM_{2.5} mass, OC and EC observed during the polluted period was characterized by low
321 wind speed but not significantly sensitive by the temperature and relative humidity.](#)

322 **3.2 Best estimate of source apportionment results**

323 **3.2.1 Fossil and biomass burning EC**

324 Figure 2 shows the source apportionment results of EC. The concentration of EC from fossil-
325 fuel sources (EC_f) ranged from 0.61 to 16.8 µg/m³, whereas the corresponding range for EC from
326 biomass burning (EC_{bb}) was 0.57 to 4.71 µg/m³. EC_f values were on average 3 times as high as
327 EC_{bb}, corresponding to a mean fraction of EC_f to total EC of 0.75. The highest concentrations of
328 EC_{bb} and EC_f were observed in Xian, followed by Beijing and the two southern sites Shanghai
329 and Guangzhou.

330 Despite the wide range of EC concentrations, the fraction of EC_f to total EC in Xian, Beijing
331 and Shanghai was fairly constant with average values of 78±3%, 76±4% and 79±4%,
332 respectively. This finding suggests that the increase of EC_f and EC_{bb} emissions in the three cities
333 on the heavily polluted days is likely due to an equal enhancement of fossil fuel and biomass-
334 burning combustion emissions and the accumulation of these particulate pollutants. At
335 Guangzhou, however, the EC_f contribution was noticeably higher on the heavily (i.e. 80±2%)
336 compared to the moderately polluted days (i.e. 57±5%), indicating that the increase of the EC
337 concentrations was rather caused by additional fossil-fuel emissions than by biomass burning.

338 The measured fossil contributions to EC correspond to those previously reported at 3 city sites
339 and 2 regional sites in China (Chen et al., 2013), but are higher than for the Maldives (31±5%),
340 India (36±3%) (Gustafsson et al., 2009) and a background site on the South Chinese island
341 Hainan (25-56%) (Zhang et al., 2014a).

342 **3.2.2 Fossil and non-fossil OC**

343 The concentration of OC from fossil-fuel sources (OC_f) ranged from 2.53 to 61.3 $\mu\text{g}/\text{m}^3$,
344 whereas the corresponding range for OC from non-fossil sources (OC_{nf}) was 0.8 to 42.7 $\mu\text{g}/\text{m}^3$
345 (Figure 3). Similar to EC, the highest mean concentrations of OC_f and OC_{nf} were both observed at
346 Xian and Beijing. The mean concentration of OC_{nf} was higher than that of OC_f for all sites except
347 Beijing. OC_f contributions (mean ± standard deviation) to total OC were 37±3%, 58±5%, 49±2%
348 and 35±8% in Xian, Beijing, Shanghai and Guangzhou, respectively, which was lower than the
349 corresponding EC_f fraction to EC for all samples (Figure 2). The high percentage of OC_{nf}
350 demonstrates that even in densely populated and urbanized areas of China, non-fossil sources are
351 still a considerable and sometimes even a dominant contributor of OC, at least in winter. The
352 large variability of the fraction of OC_f to total OC among the different cities furthermore reflects
353 complex sources and formation processes of OC_f . In addition, the ratio of EC_f to OC_f ($(EC/OC)_f$) in
354 Beijing (0.24±0.10) was substantially lower than in Xian (0.53±0.15), Shanghai (0.47±0.11) and
355 Guangzhou (0.56±0.11), which will be discussed below.

356 **3.2.3 Other biomass-burning markers**

357 Figure 4 shows that levoglucosan (lev) and mannosan (man) concentrations significantly
358 correlated with EC_{bb} . Their correlation coefficients were 0.87 and 0.92, respectively. In spite of
359 different concentration levels, no significant differences were observed in the slopes among
360 different cities for the different anhydrosugars or pollution levels. A possible explanation is that
361 the burning conditions and fuel type was rather consistent during the sampling period for the four
362 cities. Moreover, the regression slope (0.41±0.03) of levoglucosan and EC_{bb} obtained here was
363 similar to that (0.45) calculated by the ratio of the best estimates of lev/OC (0.10) and EC/OC
364 (0.22) using the LHS simulation (median values in Table 2), indicating that our assumption of
365 LHS input parameters is reasonable. The average lev-to-man ratio was 27.7 ± 8.47 (ranging from
366 16.4 to 45.9), which is at the higher end of the reported ratios for crop residue burning (ranging
367 from 12.9 to 55.7 with a mean of 32.6 ± 19.1) and obviously higher than that from softwood $4.0 \pm$
368 1.0 (ranging from 2.5 to 5.8 with a mean of 4.0 ± 1.0) (Sang et al., 2013). However, the ratio is
369 not significantly different from ratios reported for hardwood burning (ranging from 12.9 to 35.4
370 with a mean of 21.5 ± 8.3) (Sang et al., 2013).

371 Recently, Cheng et al. (2013) proposed that ratios of levoglucosan to another biomass
372 burning marker, non-sea-salt-potassium ($nss-K^+ = K^+ - 0.0355 \times Na^+$, (Lai et al., 2007)), can be
373 used to distinguish biomass burning from crop residue and wood. The average of lev-to- K_{nss}^+ in
374 our study was 0.59 ± 0.33 (ranging from 0.17 to 1.56 with only 2 samples >1), which is
375 comparable to the ratios for wheat straw (0.10 ± 0.00), corn straw (0.21 ± 0.08) and rice straw
376 grown in Asia (0.62 ± 0.32) (Cheng et al., 2013). These ratios are much lower than those ratios
377 reported for hardwood (23.96 ± 1.82) (Cheng et al., 2013). With a combination of the lev-to-man
378 and lev-to- K^+ ratios, it can be concluded that the major source of biomass burning in winter of
379 China is combustion of crop residues. In addition, non-sea-salt-potassium concentrations also
380 show a very good correlation ($R^2=0.82$) with EC_{bb} for the four cities. This also confirms that the
381 variability of burning conditions and biomass types was rather small during winter 2013 in
382 different regions of China.

383 **3.2.4 Sensitivity analysis**

384 Figure 5 shows the results of the sensitivity test for the average contribution of each source
385 to TC for all sites. Each source is illustrated as a frequency distribution, from which the
386 uncertainties of the source apportionment are deduced as given in Section 2.5. We found that
387 EC_{bb} was always the smallest contributor ($<10\%$), but was still non-negligible for all sites. The
388 distributions of EC_f and EC_{bb} were much narrower than for the different OC sources due to the
389 direct ^{14}C determination of EC and the indirect calculation of the OC fractions. OC_{bb} and $OC_{other,nf}$
390 were the most uncertain contributors to TC due to the large variation of the input parameters for
391 LHS calculations, i.e. $(EC/OC)_{bb}$ and $(lev/OC)_{bb}$. **Despite a large spread of $OC_{sec,f}$ and $OC_{other,nf}$,
392 the data conclusively shows that both contributions were always larger on the heavily than on the
393 moderately polluted days, highlighting the importance of fossil-derived SOC formation and other
394 non-fossil emissions excluding primary biomass burning sources. The increased $OC_{other,nf}$ is likely
395 due to enhanced SOC formation from biomass burning and other non-fossil sources (see Sec.
396 3.3).**

397 **3.3 The relevance of SOC for heavily polluted days**

398 **3.3.1 Further source apportionment of OC sources**

399 As explained in Sec. 2.4, OC_f is apportioned into primary and secondary OC from fossil
400 sources, whereas OC_{nf} is subdivided into primary biomass-burning OC (OC_{bb}) and the other non-
401 fossil OC ($OC_{other,nf}$). As shown in Figure 6, $OC_{sec,f}$ was generally more abundant than $OC_{pri,f}$,
402 suggesting that SOC is the predominant fraction of OC_f in Chinese cities during winter. The

403 highest $OC_{\text{sec},f}$ -to- $OC_{\text{pri},f}$ ratio (with average of 4.2) was found in Beijing, indicating the largest
404 SOC formation compared to the other three sites (average $OC_{\text{sec},f}$ -to- $OC_{\text{pri},f}$ ratio of 1.3), which is
405 in agreement with the higher OC_f/EC_f ratios (see Sect. 3.2.2). During heavily polluted days,
406 $OC_{\text{sec},f}$ -to- $OC_{\text{pri},f}$ ratios increased compared to moderately polluted days on average by 70% for
407 the 4 sites. This underlines that the episodes with bad air quality were mainly caused by
408 additional SOC formation and accumulation of similar pollutants as for average winter
409 conditions. The importance of fossil-derived SOC formation was also underlined by ^{14}C
410 measurement in water-soluble OC during 2011 winter in Beijing and Guangzhou (Zhang et al.,
411 2014b). Figure 6 shows that OC_{bb} was higher than $OC_{\text{other,nf}}$ on the moderately polluted days for
412 all sites, while it changed to the contrary on the heavily polluted days. The excess of non-fossil
413 OC concentration for the heavily polluted days was dominated by $OC_{\text{other,nf}}$, which was ~2.6 times
414 as high as OC_{bb} . The dominating contribution of $OC_{\text{other,nf}}$ is likely due to the increase of SOC
415 formation from non-fossil sources mainly from biomass-burning emissions, although biogenic-
416 derived SOC could not be excluded for SH and GZ where temperatures during the sampling
417 period are above 0 degrees. In conclusion, the source apportionment results of the excess
418 carbonaceous aerosols consistently highlight the importance of SOC from both, fossil and non-
419 fossil sources. It should be also noted that the condensation of semi-volatile organic aerosols
420 generally may contribute to some extent to the measured SOA in winter due to the colder
421 temperature in the northern sites such as Beijing and Xian. However, the increased SOA between
422 the MPD and HPD measured by the current method is mostly if not exclusively due to enhanced
423 SOA formation since the temperatures during the moderately and heavily polluted days were not
424 significantly different ($p < 0.05$).

425 **3.3.2 Relative contribution from OC and EC source categories to TC**

426 The contributions of different OC and EC source categories to TC are shown in Table 4.
427 Fossil sources ($EC_f + OC_{\text{pri},f} + OC_{\text{sec},f}$) account for an important contribution at all sites, which
428 decreased from Beijing (60%) to Shanghai (56%), Xian (45%) and Guangzhou (43%). The larger
429 fossil contribution in Beijing can be explained by substantially higher $OC_{\text{sec},f}$ values, which were
430 often >2 times as high as for the other three sites. However, no remarkable difference was found
431 for the total primary fossil contribution ($EC_f + OC_{\text{pri},f}$) between the heavily and the moderately
432 polluted days. An exception of this tendency was observed for Guangzhou, in which the fossil
433 contribution to TC increased by 36% during the polluted episodes. However, the contribution of
434 $OC_{\text{sec},f}$ to TC was higher on the heavily polluted days than on the moderately polluted days for all
435 sites, which indicates a significant contribution of fossil SOC to TC during winter haze or smog
436 episodes in China.

437 Primary biomass-burning sources ($EC_{bb}+OC_{bb}$) were a large contributor to TC (on average
438 25%, 21%, 26% and 39% in Xian, Beijing, Shanghai and Guangzhou, respectively). However, the
439 relative contribution of biomass burning decreased on average from $\sim 28\%$ to $\sim 17\%$ when
440 comparing moderately with heavily polluted days. Therefore, primary biomass-burning emissions
441 were not a major additional source during heavily polluted days.

442 A considerable fraction of TC originated from $OC_{other,nf}$ with a mean contribution of 21% for
443 all sites. The presence of $OC_{other,nf}$ is unlikely attributed to primary or secondary biogenic particles
444 as biogenic emissions are very low during winter at least in Northern China, although these can
445 be enriched due to favoring condensation of SVOCs into the particle phase at colder
446 temperatures. In combination with the observation of enhanced fossil SOC formation, we assume
447 that this excess is mainly attributed to SOC formation from non-fossil, but non-biogenic
448 precursors (i.e. mainly from biomass-burning emissions). Further, SOC formation from these
449 non-fossil volatile organic compounds may be enhanced, when they are mixed with
450 anthropogenic pollutants such as volatile organic compounds (VOCs) and NO_x (Weber et al.,
451 2007; Hoyle et al., 2011).

452 As the $OC_{sec,f}$ and $OC_{other,nf}$ contributions were always considerably higher on the most
453 polluted days compared the moderately polluted days and the increase of primary sources (such
454 as EC_{bb} , OC_{bb} and $OC_{pri,f}$) was less prominent (see Figure 6), we conclude that the increment of
455 TC on the heavily polluted days was mainly driven by the increase of SOC from both fossil fuel
456 and non-fossil emissions. This is also underlined in Figure 6 by the composition of the excess for
457 the heavily polluted days.

458 **3.3.3 Comparison with multi-linear engine (ME-2) source apportionment**

459 In a parallel study from the same sites and episodes (Huang et al., 2014), the multi-linear
460 engine (ME-2) receptor model (Canonaco et al., 2013) was used to estimate the OC contribution
461 from different factors including coal, traffic, dust-related, cooking and secondary sources. This
462 model includes EC/OC, ions and organic marker compounds (polycyclic aromatic hydrocarbons
463 (PAHs), oxygenated PAHs (o-PAHs), resin acids, anhydrous sugars, lignin pyrolysis products and
464 hopanes) in addition to high resolution Aerodyne aerosol mass spectra from offline analysis of
465 nebulized water-extracts from filter samples by a high-resolution time-of-flight aerosol mass
466 spectrometer, HR-ToF-AMS (Daellenbach et al., *in preparation*). For comparison with the results
467 from this work, sources resolved by the ME-2 approach are further classified into the following
468 basic classes: fossil primary OC (POC_f), non-fossil primary OC (POC_{nf}), fossil secondary OC
469 (SOC_f) and non-fossil secondary OC (SOC_{nf}). Figure 7 shows a significant linear correlation
470 between the two approaches ($p < 0.01$, $n = 24$, all samples are included), underscoring the proper

471 choices of the selected source profiles in this study (i.e. inputs for LHS). A very good agreement
472 between the two methods is found for SOC_{nf} , whereas an deviation of $\sim 13\%$ occurs for SOC_f
473 possibly due to uncertainties in both models. It is important to note that such a difference is not
474 observed ($p < 0.01$), if we exclude the data from Beijing. And SOC_f may be overestimated, if we
475 underestimate the contribution of coal combustion to fossil-fuel derived EC (p in Eq. (8)) in
476 Beijing. The findings of Huang et al. (2014) suggest that coal combustion is substantially higher
477 in this city compared to the other sites. Increasing the value of p by a factor of 2 (i.e. from 0.35 to
478 0.70) for Beijing decreases the contribution of SOC_f to the benefit of POC_f , whereas the other
479 components (EC_f , EC_{bb} , OC_{bb} , $\text{OC}_{\text{other,nf}}$) are independent of the choice of the p value (see Tab. S2
480 and Fig. S1). This modification improves the agreement of SOC_f between both approaches as
481 shown in Fig. 7. Furthermore, it decreases the $\text{OC}_{\text{sec,f-to-OC}_{\text{pri,f}}}$ ratio of Beijing from 2.7 and 5.9
482 to 1.2 and 2.9 for the moderately and heavily polluted days, respectively. As a consequence, these
483 values become better comparable with those of the other cities, but still underline the importance
484 of secondary aerosol formation during the heavily polluted days.

485 **4 Conclusions**

486 Source apportionment of the carbonaceous aerosol in PM_{2.5} during a severe winter pollution
487 episode of 2013 in China was conducted at four major cities including Xian, Beijing, Shanghai
488 and Guangzhou. Statistical analysis of concentrations of OC and EC, anhydrosugars as well as
489 ¹⁴C contents of OC and EC using Latin-hypercube sampling (LHS) allowed a quantitative
490 estimation of six different sources. These sources included EC from combustion of biomass
491 (EC_{bb}) and fossil fuels (EC_f), OC from fossil emissions including primary and secondary sources
492 (i.e. $\text{OC}_{\text{pri,f}}$ and $\text{OC}_{\text{sec,f}}$, respectively) as well as OC from non-fossil sources including primary
493 biomass burning and all the other non-fossil OC (i.e. OC_{bb} and $\text{OC}_{\text{other,nf}}$, respectively). A sensitivity
494 analysis of the LHS simulation showed the robustness of our results, as the uncertainty of the
495 different emission sources was usually below 20% of TC, which was mainly achieved by the
496 combination of different isotopic and molecular markers.

497 Fossil emissions predominated EC with a mean contribution of $75 \pm 8\%$ at all sites. The
498 remaining $25 \pm 8\%$ was attributed to biomass-burning sources, and the presence of the latter was
499 also confirmed by other biomass-burning markers such as levoglucosan and water-soluble
500 potassium. The fossil contribution to OC was lower than for EC and was highest in Beijing
501 ($58 \pm 5\%$) and decreased in the order: Shanghai ($49 \pm 2\%$) > Xian ($38 \pm 3\%$) > Guangzhou ($35 \pm 7\%$).

502 Conversely, non-fossil sources accounted on the average for $55 \pm 10\%$ and $48 \pm 9\%$ of OC and
503 TC, respectively. Air pollution from the neighboring rural regions may have contributed

504 substantially to non-fossil carbon of urban aerosols, as biofuel usage is more common for heating
505 and cooking in such regions during winter time in China. The average contribution of non-fossil
506 OC from OC_{bb} was found to 40±8%, 48±18%, 53±4% and 65±26% for Xian, Beijing, Shanghai
507 and Guangzhou, respectively.

508 A considerable fraction of OC was identified as SOC. We found that OC_{sec,f} dominated over
509 OC_{pri,f} for all samples (i.e. portions of TC of 23±11% compared to 13±3%, respectively), strongly
510 implying importance of fossil-derived SOC to urban (often polluted) aerosols in China.
511 Furthermore, we classified the samples into 2 episodes, heavily polluted and moderately polluted
512 days, depending on PM mass. We found the relative OC_{other,nf} contributions tend to be higher on
513 the heavily polluted days at all sites, which were mainly attributed to enhanced SOC formation
514 from non-fossil precursors such as biomass-burning emissions. Even though a significant increase
515 of absolute mass concentrations of primary emissions (both fossil and non-fossil sources) was
516 found on the heavily compared to moderately polluted days, their relative contribution to TC was
517 even decreased, while SOC contributions from both fossil and non-fossil sources were
518 substantially increased. This finding was consistently observed for all sites, showing the
519 importance of SOC during severe haze events in China.

520 **Acknowledgement**

521 Yanlin Zhang acknowledges partial support from the Swiss National Science Foundation
522 Fellowship.

523 **References**

- 524 Bernardoni, V., Calzolari, G., Chiari, M., Fedi, M., Lucarelli, F., Nava, S., Piazzalunga, A.,
525 Riccobono, F., Taccetti, F., Valli, G., and Vecchi, R.: Radiocarbon analysis on organic and
526 elemental carbon in aerosol samples and source apportionment at an urban site in Northern
527 Italy, *J. Aerosol Sci.*, 56, 88-99, 2013.
- 528 Canonaco, F., Crippa, M., Slowik, J. G., Baltensperger, U., and Prévôt, A. S. H.: SoFi, an IGOR-
529 based interface for the efficient use of the generalized multilinear engine (ME-2) for the
530 source apportionment: ME-2 application to aerosol mass spectrometer data, *Atmos. Meas.*
531 *Tech.*, 6, 3649-3661, 2013.
- 532 Cao, F., Zhang, Y.-L., Szidat, S., Zapf, A., Wacker, L., and Schwikowski, M.: Microgram level
533 radiocarbon determination of carbonaceous particles in firn samples: pre-treatment and
534 OC/EC separation, *Radiocarbon*, 55, 383-390 2013.

535 Cao, G. L., Zhang, X. Y., Gong, S. L., An, X. Q., and Wang, Y. Q.: Emission inventories of
536 primary particles and pollutant gases for China, *Chin. Sci. Bull.*, 56, 781-788, 2011a.

537 Cao, J.-j., Chow, J. C., Tao, J., Lee, S.-c., Watson, J. G., Ho, K.-f., Wang, G.-h., Zhu, C.-s., and
538 Han, Y.-m.: Stable carbon isotopes in aerosols from Chinese cities: Influence of fossil fuels,
539 *Atmos. Environ.*, 45, 1359-1363, 2011b.

540 Cao, J. J., Lee, S. C., Chow, J. C., Watson, J. G., Ho, K. F., Zhang, R. J., Jin, Z. D., Shen, Z. X.,
541 Chen, G. C., Kang, Y. M., Zou, S. C., Zhang, L. Z., Qi, S. H., Dai, M. H., Cheng, Y., and Hu,
542 K.: Spatial and seasonal distributions of carbonaceous aerosols over China, *J. Geophys. Res.*,
543 112, D22S11, 2007.

544 Cao, J. J., Shen, Z. X., Chow, J. C., Watson, J. G., Lee, S. C., Tie, X. X., Ho, K. F., Wang, G. H.,
545 and Han, Y. M.: Winter and summer PM_{2.5} chemical compositions in fourteen chinese cities,
546 *J. Air Waste Manage. Assoc.*, 62, 1214-1226, 2012.

547 Carlton, A. G., Wiedinmyer, C., and Kroll, J. H.: A review of Secondary Organic Aerosol (SOA)
548 formation from isoprene, *Atmos. Chem. Phys.*, 9, 4987-5005, 2009.

549 Cavalli, F., Viana, M., Yttri, K. E., Genberg, J., and Putaud, J. P.: Toward a standardised thermal-
550 optical protocol for measuring atmospheric organic and elemental carbon: the EUSAAR
551 protocol, *Atmos. Meas. Tech.*, 3, 79-89, 2010.

552 Chan, C. K., and Yao, X.: Air pollution in mega cities in China, *Atmos. Environ.*, 42, 1-42, 2008.

553 Chen, B., Andersson, A., Lee, M., Kirillova, E. N., Xiao, Q., Krusa, M., Shi, M., Hu, K., Lu, Z.,
554 Streets, D. G., Du, K., and Gustafsson, O.: Source forensics of black carbon aerosols from
555 china, *Environ. Sci. Technol.*, 47, 9102-9108, 2013.

556 Cheng, Y., Engling, G., He, K. B., Duan, F. K., Ma, Y. L., Du, Z. Y., Liu, J. M., Zheng, M., and
557 Weber, R. J.: Biomass burning contribution to Beijing aerosol, *Atmos. Chem. Phys.*, 13,
558 7765-7781, 2013.

559 Donkelaar, A. v., Martin, R. V., Brauer, M., Kahn, R., Levy, R., Verduzco, C., and Villeneuve, P.
560 J.: Global estimates of ambient fine particulate matter concentrations from satellite-based
561 aerosol optical depth: development and application, *Environ. Health Perspect.*, 118, 847,
562 2010.

563 Fine, P. M., Cass, G. R., and Simoneit, B. R. T.: Chemical characterization of fine particle
564 emissions from the wood stove combustion of prevalent United States tree species, *Environ.*
565 *Eng. Sci.*, 21, 705-721, 2004.

566 Gelencsér, A., May, B., Simpson, D., Sánchez-Ochoa, A., Kasper-Giebl, A., Puxbaum, H.,
567 Caseiro, A., Pio, C., and Legrand, M.: Source apportionment of PM_{2.5} organic aerosol over
568 Europe: Primary/secondary, natural/anthropogenic, and fossil/biogenic origin, *J. Geophys.*

569 Res., 112, D23S04, 2007.

570 Genberg, J., Hyder, M., Stenström, K., Bergström, R., Simpson, D., Fors, E., Jönsson, J. Å., and
571 Swietlicki, E.: Source apportionment of carbonaceous aerosol in southern Sweden, *Atmos.*
572 *Chem. Phys.*, 11, 11387-11400, 2011.

573 Gilardoni, S., Vignati, E., Cavalli, F., Putaud, J. P., Larsen, B. R., Karl, M., Stenström, K.,
574 Genberg, J., Henne, S., and Dentener, F.: Better constraints on sources of carbonaceous
575 aerosols using a combined ¹⁴C-macro tracer analysis in a European rural background site,
576 *Atmos. Chem. Phys.*, 11, 5685-5700, 2011.

577 Gustafsson, O., Krusa, M., Zencak, Z., Sheesley, R. J., Granat, L., Engstrom, E., Praveen, P. S.,
578 Rao, P. S., Leck, C., and Rodhe, H.: Brown clouds over South Asia: biomass or fossil fuel
579 combustion?, *Science*, 323, 495-498, 2009.

580 He, L. Y., Hu, M., Zhang, Y. H., Huang, X. F., and Yao, T. T.: Fine particle emissions from on-
581 road vehicles in the Zhujiang Tunnel, China, *Environ. Sci. Technol.*, 42, 4461-4466, 2008.

582 Heal, M.: The application of carbon-14 analyses to the source apportionment of atmospheric
583 carbonaceous particulate matter: a review, *Anal. Bioanal. Chem.*, 406, 81-98, 2014.

584 Hoyle, C. R., Boy, M., Donahue, N. M., Fry, J. L., Glasius, M., Guenther, A., Hallar, A. G., Hartz,
585 K. H., Petters, M. D., Petaja, T., Rosenoern, T., and Sullivan, A. P.: A review of the
586 anthropogenic influence on biogenic secondary organic aerosol, *Atmos. Chem. Phys.*, 11,
587 321-343, 2011.

588 Huang, K., Zhuang, G., Lin, Y., Wang, Q., Fu, J. S., Fu, Q., Liu, T., and Deng, C.: How to
589 improve the air quality over megacities in China: pollution characterization and source
590 analysis in Shanghai before, during, and after the 2010 World Expo, *Atmos. Chem. Phys.*, 13,
591 5927-5942, 2013.

592 Huang, R.-J., Zhang, Y., Bozzetti, C., Ho, K.-F., Cao, J., Han, Y., Dällenbach, K. R., Slowik, J.
593 G., Platt, S. M., Canonaco, F., Zotter, P., Wolf, R., Pieber, S. M., Bruns, E. A., Crippa, M.,
594 Ciarelli, G., Piazzalunga, A., Schwikowski, M., Abbaszade, G., Schnelle-Kreis, J.,
595 Zimmermann, R., An, Z., Szidat, S., Baltensperger, U., Haddad, I. E., and Prévôt, A. S. H.:
596 High secondary aerosol contribution to particulate pollution during haze events in China,
597 *Nature*, *In press*, 2014.

598 Huang, X. F., Yu, J. Z., He, L. Y., and Hu, M.: Size distribution characteristics of elemental
599 carbon emitted from Chinese vehicles: Results of a tunnel study and atmospheric
600 implications, *Environ. Sci. Technol.*, 40, 5355-5360, 2006.

601 IPCC: Climate change 2013: The physical science basis. contribution of working group I to the
602 fifth assessment report of the intergovernmental panel on climate change, Cambridge

603 University Press, Cambridge, United Kingdom and New York, NY, USA, 1533 pp., 2013.

604 Lai, S. c., Zou, S. c., Cao, J. j., Lee, S. c., and Ho, K. f.: Characterizing ionic species in PM_{2.5} and
605 PM₁₀ in four Pearl River Delta cities, South China, *Journal of Environmental Sciences*, 19,
606 939-947, 2007.

607 Levin, I., Naegler, T., Kromer, B., Diehl, M., Francey, R. J., Gomez-Pelaez, A. J., Steele, L. P.,
608 Wagenbach, D., Weller, R., and Worthy, D. E.: Observations and modelling of the global
609 distribution and long-term trend of atmospheric ¹⁴CO₂, *Tellus Series B*, 62, 26-46, 2010.

610 Liu, D., Li, J., Zhang, Y., Xu, Y., Liu, X., Ding, P., Shen, C., Chen, Y., Tian, C., and Zhang, G.:
611 The use of levoglucosan and radiocarbon for source apportionment of PM_{2.5} carbonaceous
612 aerosols at a background site in East China, *Environ. Sci. Technol.*, 47, 10454-10461, 2013.

613 Minguillón, M. C., Perron, N., Querol, X., Szidat, S., Fahrni, S. M., Alastuey, A., Jimenez, J. L.,
614 Mohr, C., Ortega, A. M., Day, D. A., Lanz, V. A., Wacker, L., Reche, C., Cusack, M., Amato,
615 F., Kiss, G., Hoffer, A., Decesari, S., Moretti, F., Hillamo, R., Teinila, K., Seco, R., Penuelas,
616 J., Metzger, A., Schallhart, S., Muller, M., Hansel, A., Burkhardt, J. F., Baltensperger, U., and
617 Prevot, A. S. H.: Fossil versus contemporary sources of fine elemental and organic
618 carbonaceous particulate matter during the DAURE campaign in Northeast Spain, *Atmos.*
619 *Chem. Phys.*, 11, 12067-12084, 2011.

620 Mohn, J., Szidat, S., Fellner, J., Rechberger, H., Quartier, R., Buchmann, B., and Emmenegger,
621 L.: Determination of biogenic and fossil CO₂ emitted by waste incineration based on ¹⁴CO₂
622 and mass balances, *Bioresour. Technol.*, 99, 6471-6479, 2008.

623 Nordin, E., Eriksson, A., Roldin, P., Nilsson, P., Carlsson, J., Kajos, M., Hellén, H., Wittbom, C.,
624 Rissler, J., and Löndahl, J.: Secondary organic aerosol formation from idling gasoline
625 passenger vehicle emissions investigated in a smog chamber, *Atmos. Chem. Phys.*, 13, 6101-
626 6116, 2013.

627 Orasche, J., Schnelle-Kreis, J., Abbaszade, G., and Zimmermann, R.: Technical Note: In-situ
628 derivatization thermal desorption GC-TOFMS for direct analysis of particle-bound non-polar
629 and polar organic species, *Atmos. Chem. Phys.*, 11, 8977-8993, 2011.

630 Paatero, P., and Tapper, U.: Positive matrix factorization - A nonnegative factor model with
631 optimal utilization of error-estimates of data values, *Environmetricsz*, 5, 111-126, 1994.

632 Paatero, P., and Hopke, P. K.: Rotational tools for factor analytic models, *J. Chemom.*, 23, 91-
633 100, 2009.

634 Pöschl, U.: Atmospheric aerosols: composition, transformation, climate and health effects,
635 *Angew. Chem., Int. Ed.*, 44, 7520-7540, 2005.

636 Puxbaum, H., Caseiro, A., Sánchez-Ochoa, A., Kasper-Giebl, A., Claeys, M., Gelencsér, A.,

637 Legrand, M., Preunkert, S., and Pio, C.: Levoglucosan levels at background sites in Europe
638 for assessing the impact of biomass combustion on the European aerosol background, *J.*
639 *Geophys. Res.*, 112, D23S05, 2007.

640 Sang, X. F., Chan, C. Y., Engling, G., Chan, L. Y., Wang, X. M., Zhang, Y. N., Shi, S., Zhang, Z.
641 S., Zhang, T., and Hu, M.: Levoglucosan enhancement in ambient aerosol during springtime
642 transport events of biomass burning smoke to Southeast China, *Tellus Series B-Chemical and*
643 *Physical Meteorology*, 63, 129-139, 2011.

644 Sang, X. F., Zhang, Z. S., Chan, C. Y., and Engling, G.: Source categories and contribution of
645 biomass smoke to organic aerosol over the southeastern Tibetan Plateau, *Atmos. Environ.*, 78,
646 113-123, 2013.

647 Schmidl, C., Marr, I. L., Caseiro, A., Kotianová, P., Berner, A., Bauer, H., Kasper-Giebl, A., and
648 Puxbaum, H.: Chemical characterisation of fine particle emissions from wood stove
649 combustion of common woods growing in mid-European Alpine regions, *Atmos. Environ.*,
650 42, 126-141, 2008.

651 Schnelle-Kreis, J., Sklorz, M., Peters, A., Cyrus, J., and Zimmermann, R.: Analysis of particle-
652 associated semi-volatile aromatic and aliphatic hydrocarbons in urban particulate matter on a
653 daily basis, *Atmos. Environ.*, 39, 7702-7714, 2005.

654 Simoneit, B. R. T., Schauer, J. J., Nolte, C. G., Oros, D. R., Elias, V. O., Fraser, M. P., Rogge, W.
655 F., and Cass, G. R.: Levoglucosan, a tracer for cellulose in biomass burning and atmospheric
656 particles, *Atmos. Environ.*, 33, 173-182, 1999.

657 Stuiver, M., and Polach, H. A.: Discussion: Reporting of ^{14}C data, *Radiocarbon*, 19, 355-363,
658 1977.

659 Szidat, S., Jenk, T. M., Synal, H.-A., Kalberer, M., Wacker, L., Hajdas, I., Kasper-Giebl, A., and
660 Baltensperger, U.: Contributions of fossil fuel, biomass-burning, and biogenic emissions to
661 carbonaceous aerosols in Zurich as traced by ^{14}C , *J. Geophys. Res.*, 111, D07206, 2006.

662 Szidat, S., Prévôt, A. S. H., Sandradewi, J., Alfarra, M. R., Synal, H. A., Wacker, L., and
663 Baltensperger, U.: Dominant impact of residential wood burning on particulate matter in
664 Alpine valleys during winter, *Geophys. Res. Lett.*, 34, L05820, 2007.

665 Szidat, S.: Sources of Asian haze, *Science*, 323, 470-471, 2009.

666 Szidat, S., Ruff, M., Perron, N., Wacker, L., Synal, H.-A., Hallquist, M., Shannigrahi, A. S., Yttri,
667 K. E., Dye, C., and Simpson, D.: Fossil and non-fossil sources of organic carbon (OC) and
668 elemental carbon (EC) in Goeteborg, Sweden, *Atmos. Chem. Phys.*, 9, 1521-1535, 2009.

669 Szidat, S., Salazar, G. A., Vogel, E., Battaglia, M., Wacker, L., Synal, H.-A., and Türlér, A.: ^{14}C
670 Analysis and Sample Preparation at the New Bern Laboratory for the Analysis of

671 Radiocarbon with AMS (LARA), *Radiocarbon*, 56, 561-566, 2014.

672 Viana, M., Reche, C., Amato, F., Alastuey, A., Querol, X., Moreno, T., Lucarelli, F., Nava, S.,
673 Cazolai, G., Chiari, M., and Rico, M.: Evidence of biomass burning aerosols in the Barcelona
674 urban environment during winter time, *Atmos. Environ.*, 72, 81-88, 2013.

675 Wacker, L., Fahrni, S. M., Hajdas, I., Molnar, M., Synal, H. A., Szidat, S., and Zhang, Y. L.: A
676 versatile gas interface for routine radiocarbon analysis with a gas ion source, *Nucl. Instrum.*
677 *Meth. B*, 294, 315-319, 2013.

678 Weber, R. J., Sullivan, A. P., Peltier, R. E., Russell, A., Yan, B., Zheng, M., de Gouw, J., Warneke,
679 C., Brock, C., Holloway, J. S., Atlas, E. L., and Edgerton, E.: A study of secondary organic
680 aerosol formation in the anthropogenic-influenced southeastern United States, *J. Geophys.*
681 *Res.*, 112, D13302, 2007.

682 Weilenmann, M., Favez, J.-Y., and Alvarez, R.: Cold-start emissions of modern passenger cars at
683 different low ambient temperatures and their evolution over vehicle legislation categories,
684 *Atmos. Environ.*, 43, 2419-2429, 2009.

685 WHO: Air Quality Guidelines: Global Update 2005: Particulate Matter, Ozone, Nitrogen Dioxide
686 and Sulfur Dioxide, World Health Organization, 2006.

687 Yang, F., Tan, J., Zhao, Q., Du, Z., He, K., Ma, Y., Duan, F., Chen, G., and Zhao, Q.:
688 Characteristics of PM_{2.5} speciation in representative megacities and across China, *Atmos.*
689 *Chem. Phys.*, 11, 5207-5219, 2011.

690 Yttri, K. E., Simpson, D., Stenström, K., Puxbaum, H., and Svendby, T.: Source apportionment of
691 the carbonaceous aerosol in Norway-quantitative estimates based on ¹⁴C, thermal-optical and
692 organic tracer analysis, *Atmos. Chem. Phys.*, 11, 9375-9394, 2011.

693 Zhang, Q., Streets, D. G., He, K., and Klimont, Z.: Major components of China's anthropogenic
694 primary particulate emissions, *Environ. Res. Lett.*, 2, 045027, 2007.

695 Zhang, T., Claeys, M., Cachier, H., Dong, S. P., Wang, W., Maenhaut, W., and Liu, X. D.:
696 Identification and estimation of the biomass burning contribution to Beijing aerosol using
697 levoglucosan as a molecular marker, *Atmos. Environ.*, 42, 7013-7021, 2008.

698 Zhang, Y.-L., Li, J., Zhang, G., Zotter, P., Huang, R.-J., Tang, J.-H., Wacker, L., Prévôt, A. S. H.,
699 and Szidat, S.: Radiocarbon-based source apportionment of carbonaceous aerosols at a
700 regional background site on hainan Island, South China, *Environ. Sci. Technol.*, 48, 2651-
701 2659, 2014a.

702 Zhang, Y.-l., Liu, J.-w., Salazar, G. A., Li, J., Zotter, P., Zhang, G., Shen, R.-r., Schäfer, K.,
703 Schnelle-Kreis, J., Prévôt, A. S. H., and Szidat, S.: Micro-scale (μg) radiocarbon analysis of
704 water-soluble organic carbon in aerosol samples, *Atmos. Environ.*, 97, 1-5, 2014b.

705 Zhang, Y. L., Perron, N., Ciobanu, V. G., Zotter, P., Minguillon, M. C., Wacker, L., Prevot, A. S.
706 H., Baltensperger, U., and Szidat, S.: On the isolation of OC and EC and the optimal strategy
707 of radiocarbon-based source apportionment of carbonaceous aerosols, *Atmos. Chem. Phys.*,
708 12, 10841-10856, 2012.

709 Zhang, Y. L., Zotter, P., Perron, N., Prévôt, A. S. H., Wacker, L., and Szidat, S.: Fossil and non-
710 fossil sources of different carbonaceous fractions in fine and coarse particles by radiocarbon
711 measurement, *Radiocarbon*, 55, 1510-1520, 2013.

712 Zhao, P. S., Dong, F., He, D., Zhao, X. J., Zhang, X. L., Zhang, W. Z., Yao, Q., and Liu, H. Y.:
713 Characteristics of concentrations and chemical compositions for PM_{2.5} in the region of
714 Beijing, Tianjin, and Hebei, China, *Atmos. Chem. Phys.*, 13, 4631-4644, 2013.

715 Zhi, G., Chen, Y., Feng, Y., Xiong, S., Li, J., Zhang, G., Sheng, G., and Fu, J.: Emission
716 Characteristics of Carbonaceous Particles from Various Residential Coal-Stoves in China,
717 *Environ. Sci. Technol.*, 42, 3310-3315, 2008.

718 Zotter, P., El-Haddad, I., Zhang, Y., Hayes, P. L., Zhang, X., Lin, Y.-H., Wacker, L., Schnelle-
719 Kreis, J., Abbaszade, G., Zimmermann, R., Surratt, J. D., Weber, R., Jimenez, J. L., Szidat, S.,
720 Baltensperger, U., and Prévôt, A. S. H.: Diurnal cycle of fossil and non-fossil carbon using
721 radiocarbon analyses during CalNex, *J. Geophys. Res.*, 119, 6818-6835, 2014.

722 **Table 1.** Sampling information.

City	City description (population)	Location	Temperature (°C)
Xian (XA) Northern China	The largest city in Guanzhong city cluster (8.6 million)	34.2 °N, 108.9 °E	-12 – -1
Beijing (BJ) Northern China	Capital of China, developed megacity in Beijing-Tianjin- Hebei city cluster (20.7 million)	39.9 °N, 116.4 °E	-9 – -1
Shanghai (SH) Southern China	Industrial and commercial megacity in Yangtze Delta Region city cluster (24 million)	31.3 °N, 121.5 °E	2 – 11
Guangzhou (GZ) Southern China	Industrial and commercial megacity in Pearl River Delta Region city cluster (12.7 million)	23.1 °N, 113.4 °E	7 – 19

723

724 **Table 2.** Central values with low and high limits of input parameters for source apportionment using
 725 LHS

Parameter	Low	central	high
EC error factor ^a	0.75	^b	1.25
(lev/OC) _{bb}	0.07	0.11	0.20
(EC/OC) _{bb}	0.10	0.22	0.30
(EC/OC) _{pri,cc}	0.32	0.44	0.62
(EC/OC) _{pri,ve}	0.8	^b	2.1
p	0	^b	0.7
f _M (bb)	1.05	1.10	1.15
f _M (nf)	1.03	^b	^c

726 ^a EC values multiplied by given factor.

727 ^b the average of low and high limits is used.

728 ^c f_M(nf) constrained to be < f_M(bb)

729 **Table 3.** Averages and standard deviations of the mass concentrations ($\mu\text{g}/\text{m}^3$) of PM2.5, OC and EC
 730 as well as EC/OC ratios and fractions of modern (f_M) of OC and EC for samples collected on
 731 moderately polluted days (MPD) (n=3 for each city) and heavily polluted days (HPD) (n=3 for each
 732 city) in Xian, Beijing, Shanghai and Guangzhou.

	PM2.5	OC	EC	EC/OC	$f_M(\text{OC})$	$f_M(\text{EC})$
Xian						
MPD	136±27	24.6±6.3	7.2±1.9	0.30±0.07	0.67±0.04	0.25±0.03
HPD	479±25	94.2±6.8	19.8±0.9	0.21±0.02	0.66±0.02	0.24±0.02
HPD/MPD	3.5±0.7	3.8±1.0	2.7±0.7	0.71±0.17	0.99±0.06	0.98±0.16
Beijing						
MPD	85±17	18.0±3.4	4.0±0.2	0.23±0.06	0.49±0.03	0.30±0.02
HPD	266±49	59.2±7.5	7.7±0.9	0.13±0.03	0.40±0.01	0.23±0.02
HPD/MPD	3.1±0.9	3.3±0.8	1.9±0.2	0.57±0.18	0.82±0.06	0.79±0.09
Shanghai						
MPD	59±10	6.2±1.0	1.9±0.1	0.31±0.04	0.55±0.03	0.21±0.02
HPD	131±3	15.6±0.5	4.2±0.3	0.27±0.02	0.54±0.01	0.24±0.04
HPD/MPD	2.2±0.4	2.5±0.4	2.2±0.2	0.87±0.12	0.99±0.06	1.13±0.22
Guangzhou						
MPD	38±14	5.4±2.3	1.6±0.5	0.31±0.04	0.75±0.05	0.48±0.05
HPD	96±6	23.3±2.2	6.1±0.4	0.26±0.01	0.62±0.01	0.22±0.02
HPD/MPD	2.5±1.0	4.3±1.9	3.8±1.1	0.84±0.11	0.83±0.06	0.47±0.06

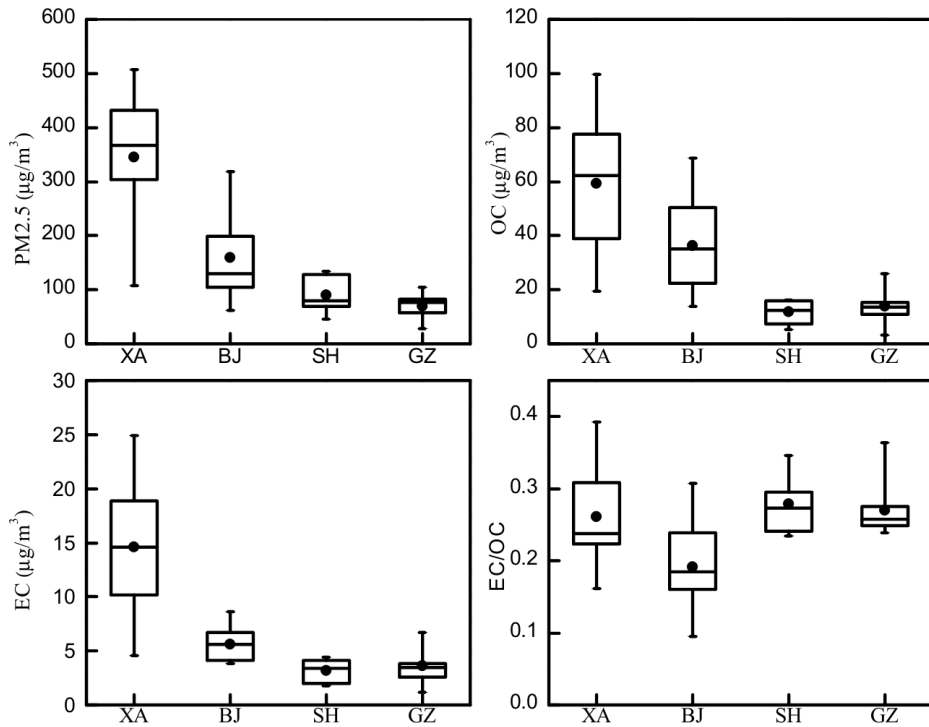
733

734 **Table 4.** Average TC concentration and relative contribution to TC from OC and EC source categories
735 (see in Figure 6) for samples collected in Xian (XA), Beijing (BJ), Shanghai (SH) and Guangzhou
736 (GZ) during the moderately polluted days (MPD) and the heavily polluted days (HPD). Distributions
737 from Latin-hypercube sampling (LHS) are given as medians as well as the 10th and 90th percentiles (in
738 parentheses). See Tab. S2 for an alternative solution for Beijing assuming a higher contribution of coal
739 combustion as explained below in Section 3.3.3.

740

Sample code	TC μg/m ³	EC _f %	EC _{bb} %	OC _{pri,f} %	OC _{sec,f} %	OC _{bb} %	OC _{other,nf} %
XA-MPD	31.8	18 (16-19)	5 (4-5)	16 (12-21)	12 (7-16)	25 (19-33)	24 (15-29)
XA-HPD	114.0	14 (12-15)	4 (3-4)	12 (10-16)	19 (15-22)	16 (13-20)	35 (30-38)
BJ-MPD	22.0	13 (12-15)	5 (4-5)	12 (9-16)	32 (27-35)	22 (17-29)	16 (8-20)
BJ-HPD	66.9	9 (8-10)	2 (2-3)	8 (6-11)	47 (44-49)	12 (9-17)	21 (16-23)
SH-MPD	8.1	19 (17-20)	5 (4-5)	17 (13-22)	21 (15-25)	23 (17-31)	16 (7-21)
SH-HPD	19.8	17 (15-18)	5 (4-5)	15 (12-20)	24 (19-28)	19 (15-24)	21 (16-25)
GZ-MPD	7.0	13 (12-15)	10 (9-11)	12 (9-16)	11 (7-14)	45 (37-52)	9 (0-17)
GZ-HPD	29.4	17 (15-18)	4 (4-5)	15 (12-20)	18 (13-22)	20 (16-27)	26 (19-30)

741



742

743

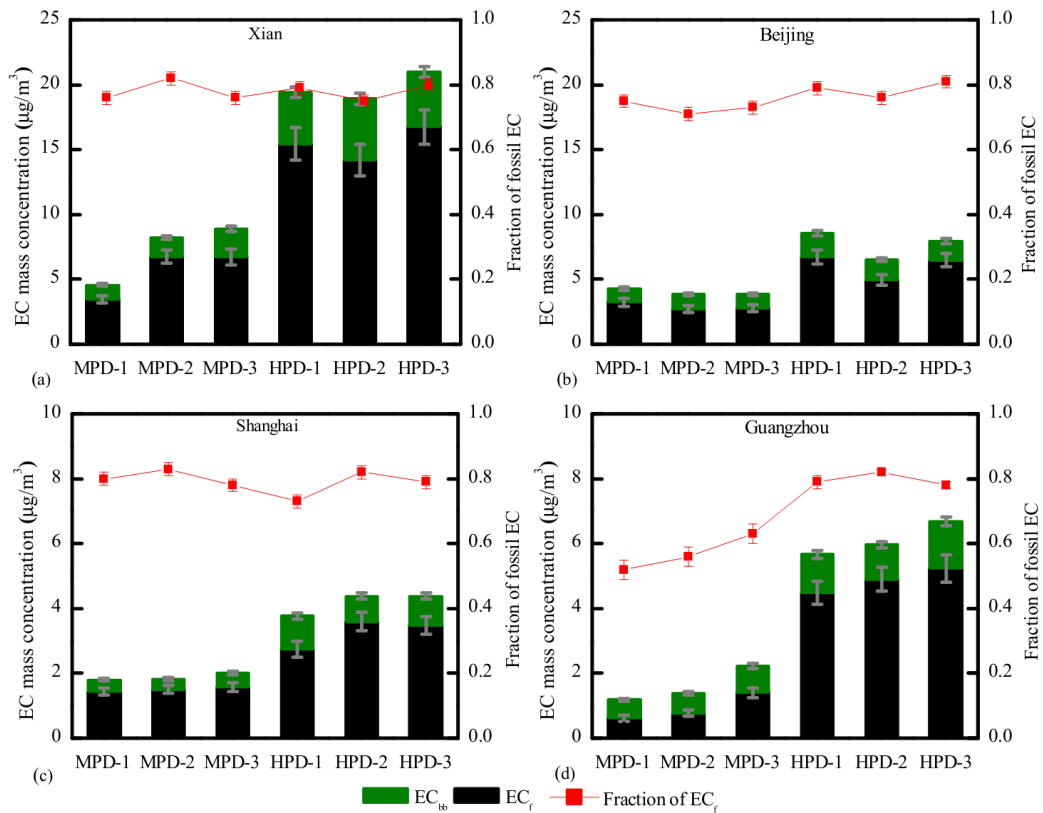
744

745

746

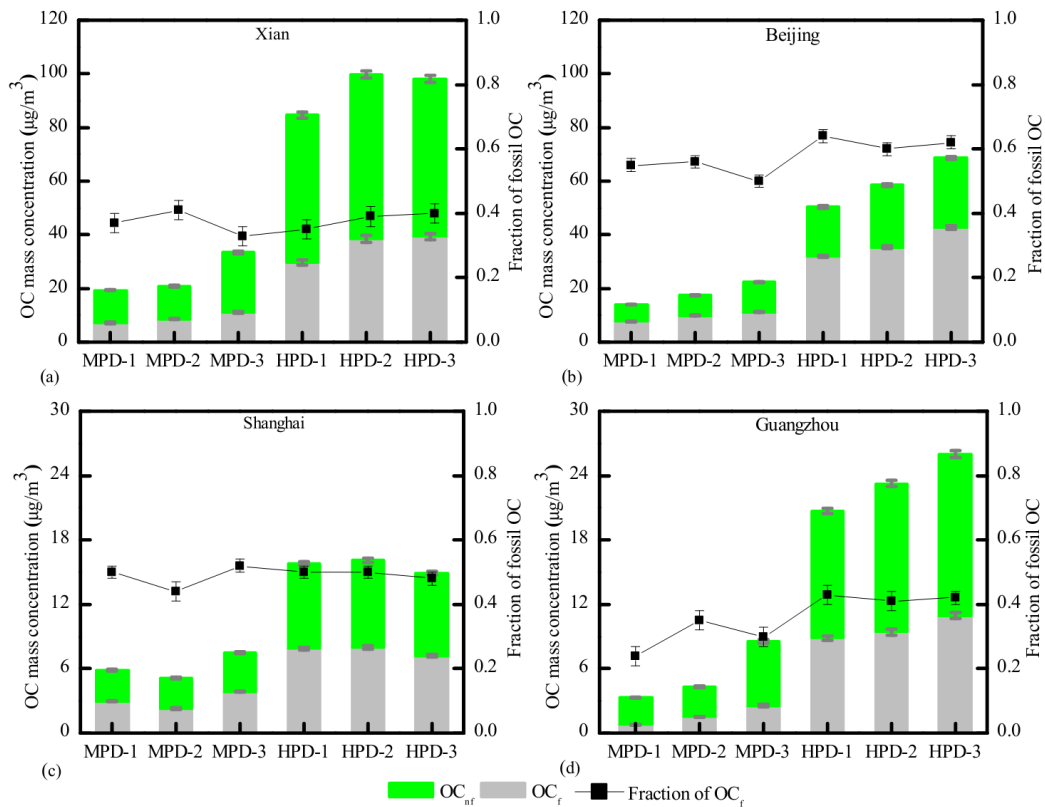
747

Figure 1. Whisker-box plots of mass concentrations of PM_{2.5} (a), OC (b) and EC (c) as well as EC/OC ratios (d) for samples collected in Xian (XA), Beijing (BJ), Shanghai (SH) and Guangzhou (GZ) during the winter of 2013. The box represents the 25th (lower line), 50th (middle line) and 75th (top line) percentiles; the solid dots within the box represent the mean values; the end of the vertical bars represents the 10th (below the box) and 90th (above the box) percentiles.



748

749 **Figure 2.** Mass concentrations ($\mu\text{g}/\text{m}^3$) of EC from biomass burning and fossil-fuel combustion (EC_{bb}
 750 and EC_f, respectively) as well as fractions of fossil EC to total EC for aerosol samples in Xian,
 751 Beijing, Shanghai and Guangzhou during moderately polluted days (MPD) and heavily polluted days
 752 (HPD). Note the different scaling for the northern and the southern cities.



753

754

Figure 3. Mass concentrations ($\mu\text{g}/\text{m}^3$) of OC from non-fossil and fossil emissions (OC_{nf} and OC_{f} ,

755

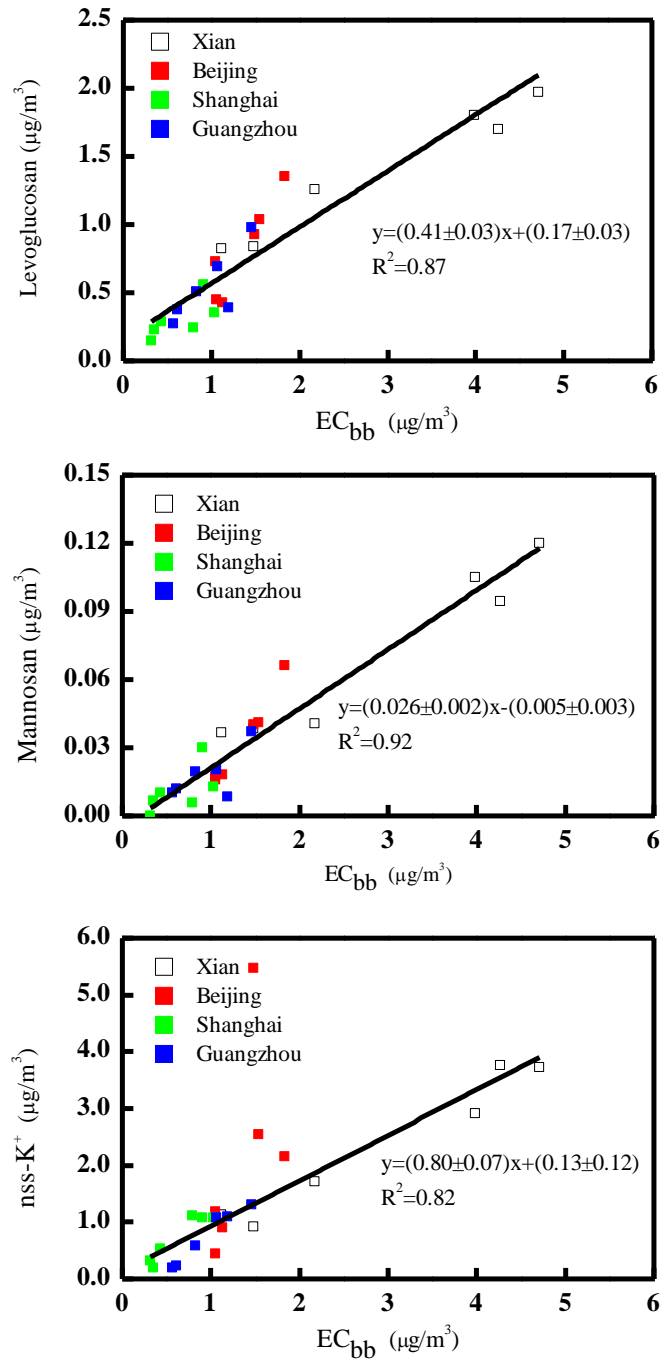
respectively) as well as fractions of fossil OC to total OC for samples collected in Xian, Beijing ,

756

Shanghai and Guangzhou during moderately polluted days (MPD) and heavily polluted days (HPD).

757

Note the different scaling for the northern and the southern cities.

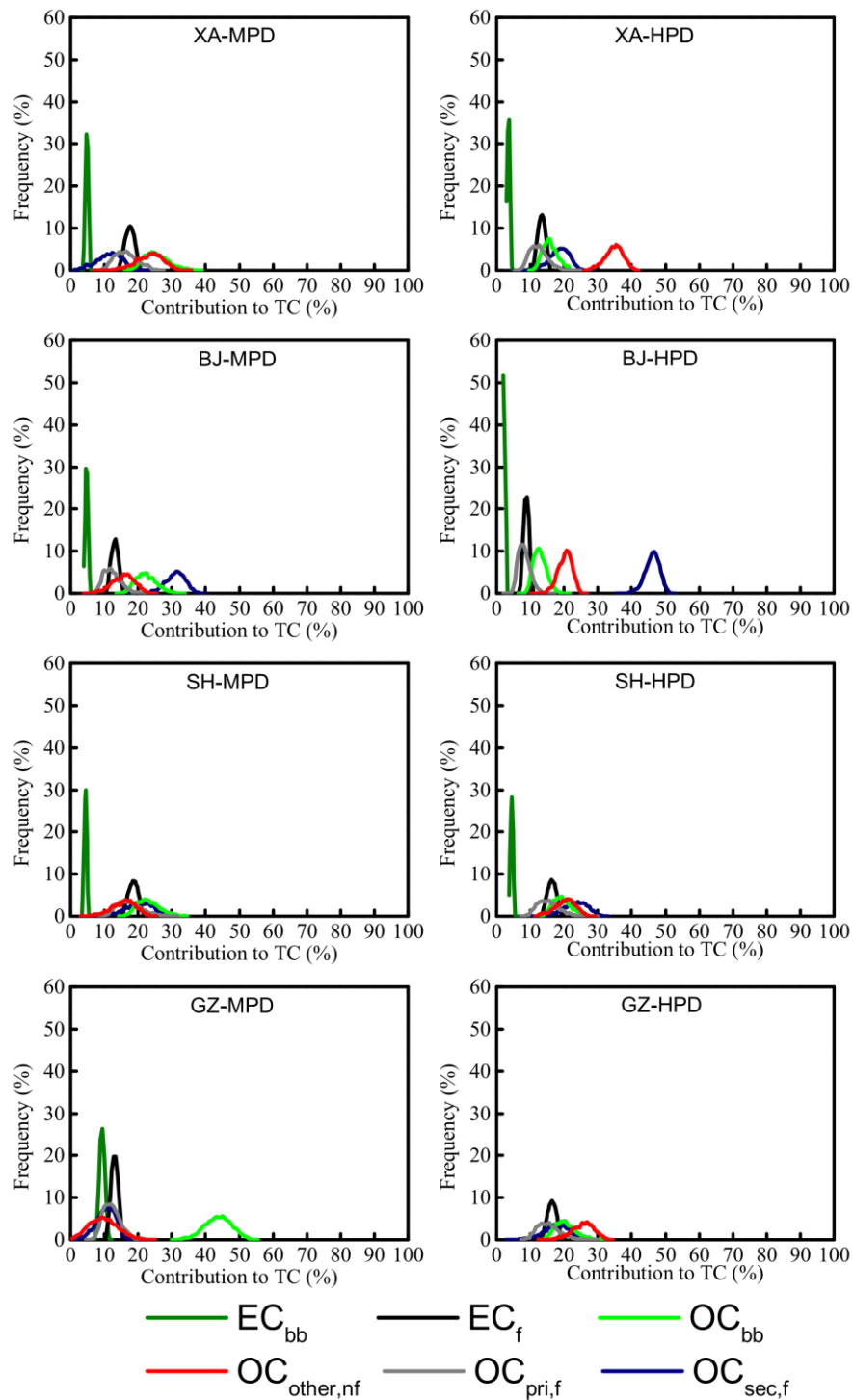


758

759 **Figure 4.** Scatter plots of concentrations of EC_{bb} with levoglucosan (top), mannosan (middle) and

760 non-sea-salt-potassium (nss-K⁺, bottom).

761

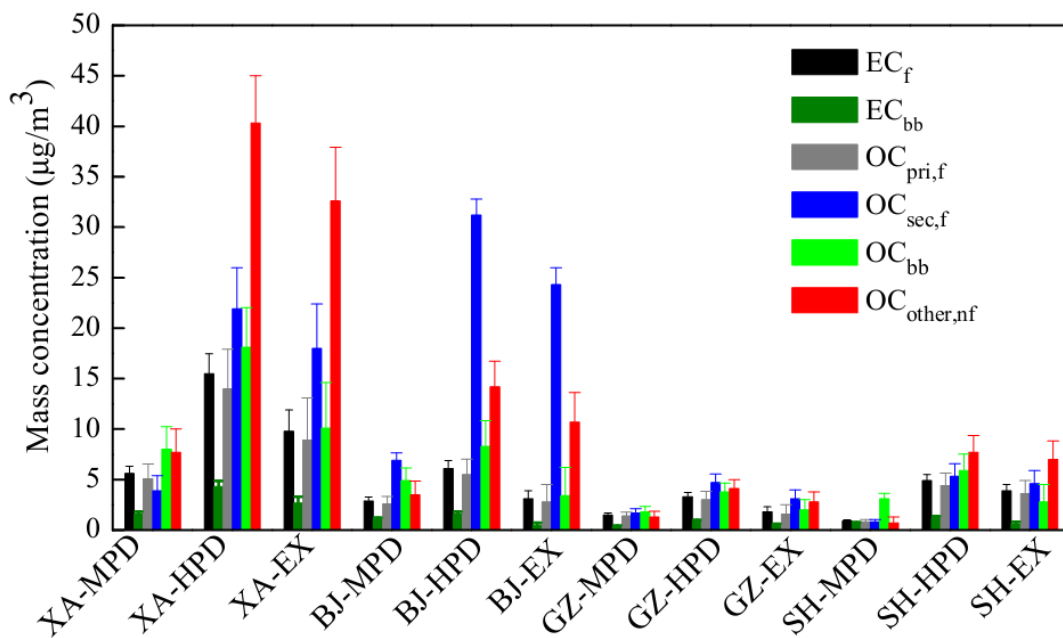


762

763

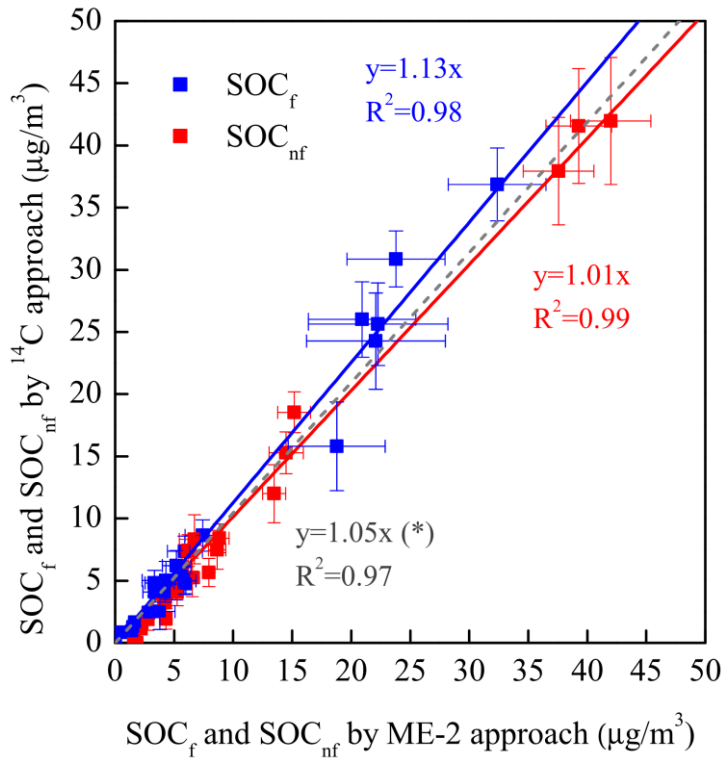
Figure 5. Latin-hypercube sampling (LHS) solutions of frequency distributions of the source contributions to TC from OC and EC source categories (see in Table 4) for samples collected in Xian (XA), Beijing (BJ), Shanghai (SH) and Guangzhou (GZ) during the moderately polluted days (MPD) and the heavily polluted days (HPD), respectively.

767



768

769 **Figure 6.** Average mass concentrations of OC and EC from different sources for samples collected in
 770 Xian (XA), Beijing (BJ), Shanghai (SH) and Guangzhou (GZ) during the moderately polluted days
 771 (MPD), heavily polluted days (HPD) and their corresponding excess (EX=HPD-MPD). Uncertainty
 772 bars represent 10 and 90 percentiles from LHS calculations. See Fig. S1 for an alternative solution for
 773 Beijing assuming a higher contribution of coal combustion as explained in Section 3.3.3.



774

775 **Figure 7.** Comparison of secondary OC from fossil and non-fossil sources (i.e. SOC_f and SOC_{nf} ,
 776 respectively) resolved by the ^{14}C and ME-2 approaches. The dashed line denotes a linear
 777 regression fit of SOC_f when excluding data from Beijing yielding an alternative regression slope
 778 marked with an asterisk (*). Note that the intercepts are insignificant for all three cases.